Structure-Based Design and Synthesis of Novel Inhibitors targeting HDAC8 from Schistosoma mansoni for the Treatment of Schistosomiasis

Tino Heimburg, Alokta Chakrabarti, Julien Lancelot, Martin Marek, Jelena Melesina, Alexander-Thomas Hauser, Tajith B Shaik, Sylvie Duclaud, Dina Robaa, Frank Erdmann, et al.

Structure-Based Design and Synthesis of Novel Inhibitors targeting HDAC8 from *Schistosoma mansoni* for the Treatment of Schistosomiasis

Tino Heimburg[1‡], Alokta Chakrabarti[2‡], Julien Lancelot[3], Martin Marek[4], Jelena Melesina[1], Alexander-Thomas Hauser[2], Tajith B. Shaik[4], Sylvie Duclaud[4], Dina Robaa[1], Frank Erdmann[1], Matthias Schmidt[1], Christophe Romier[4], Raymond J. Pierce[3], Manfred Jung[2] and Wolfgang Sippl[1*]

[1]Institute of Pharmacy, Martin-Luther University of Halle-Wittenberg, 06120 Halle/Saale, Germany

[2]Institute of Pharmaceutical Sciences, University of Freiburg, 79104 Freiburg, Germany

[3]Universite Lille, CNRS, Inserm, CHU Lille, Institut Pasteur de Lille, U1019 - UMR 8204 - CIIL - Centre d'Infection et d'Immunité de Lille, 59000 Lille, France

[4]Département de Biologie Structurale Intégrative, Institut de Génétique et Biologie Moléculaire et Cellulaire (IGBMC), Université de Strasbourg (UDS), CNRS, INSERM, 67404 Illkirch Cedex, France

[‡] These authors contributed equally to the manuscript.

KEYWORDS: *Schistosoma mansoni*, smHDAC8, histone deacetylase, co-crystallization, docking, anti-parasitic inhibitors.

ABSTRACT

Schistosomiasis is a major neglected parasitic disease that affects more than 265 million people worldwide and for which the control strategy consists of mass treatment with the only available drug, praziquantel. In this study, a series of new benzohydroxamates was prepared as potent inhibitors of *Schistosoma mansoni* histone deacetylase 8 (smHDAC8). Crystallographic analysis provided insights into the inhibition mode of smHDAC8 activity by these 3-amido-benzohydroxamates. The newly-designed inhibitors were evaluated in screens for enzyme inhibitory activity against schistosome and human HDACs. Twenty-seven compounds were found to be active in the nanomolar range and some of them showed selectivity towards smHDAC8 compared to the major human HDACs (1 and 6). The active benzohydroxamates were additionally screened for lethality against the schistosome larval stage using a fluorescence-based assay. Four of these showed significant, dose-dependent killing of the schistosome larvae and markedly impaired egg laying of adult worm pairs maintained in culture.

INTRODUCTION

Schistosomiasis is one of the major neglected parasitic diseases[1] second in importance only to malaria. It is caused by parasites from the genus *Schistosoma*[2,3], *S. mansoni* being the most widely distributed species[4]. Worldwide more than 265 million individuals are infected[5] of whom 280,000 die annually[4,6]. To date, there is no effective vaccine available and control depends on mass drug administration using the only available treatment, praziquantel, which is effective against all species of human schistosomiasis[7,8]. In 2013 over 30 million people were treated in sub-Saharan Africa[9], and this raises serious concerns about the selection of drug resistance. The reduced efficiency of praziquantel, as well as the observed resistance in laboratory strains underline the need for considering alternative therapeutic strategies[7,8,10,11]. Indeed, drug resistance represents an increasing problem for the treatment of a number of parasitic diseases for which only a few drugs are available. Thus, novel potential drug targets and drug candidates against eukaryotic parasites are urgently required[12].

Histone modifying enzymes (HMEs), which are responsible for post-translational modifications of histone and non-histone substrates, have been reported as drug targets for many diseases such as cancer, inflammation, metabolic diseases and neuropsychiatric disorders as well as in regenerative medicine[13,14,15,16]. One of the best investigated post-translational modifications is the acetylation/deacetylation of lysine residues in histone and non-histone proteins. The process of acetylation and deacetylation is controlled by histone acetyl transferases (HATs) and histone deacetylases (HDACs), respectively. The equilibrium between acetylated and non-acetylated histone proteins must be maintained for proper transcriptional activity and cellular function[17]. Additionally an increasing number of non-histone proteins have been reported as substrates of HDACs[18]. These proteins may be involved in transcription complexes, which play a pivotal role in the regulation of gene expression as well as cell proliferation, migration, death and angiogenesis[18]. HDACs are a family of

enzymes found in many organisms including bacteria, fungi, plants and animals. Eighteen different members of the HDAC family have been annotated in the human genome and have been classified into four categories based on their homology to yeast histone deacetylases[19]. Class I consists of four different subtypes (HDAC1, 2, 3 and 8) and shows homology to the yeast protein RPD3, Class II includes six subtypes which are divided into two subclasses, Class IIa with subtypes HDAC4, 5, 7 and 9, and Class IIb with HDAC6 and 10. HDAC11 is referred to as Class IV. While the activity of the enzymes belonging to Class I, II and IV HDACs depends on a zinc based catalytic mechanism, Class III enzymes, also called sirtuins, use nicotinamide adenine dinucleotide as cofactor[20]. Hereafter, the term HDAC will refer only to the classical zinc dependent deacetylases.

Numerous HDAC inhibitors (HDACi) have been identified in the last decade; several are in clinical trials and five are currently approved for the treatment of cancer, for example the aliphatic hydroxamate SAHA (Figure 1) marketed under the name Vorinostat[21,22,23,24,25,26]. The pan inhibitor SAHA is a weak inhibitor of HDAC8 (µM range). Several aromatic[27,28,29] and cinnamic acid[30]-based hydroxamates have been developed recently as selective inhibitors for the human HDAC8 (Figure 1). The indole derivative **PCI-34051**[27] represents the most selective HDAC8 inhibitor in vitro with an IC_{50} of 10 nM for HDAC8 and a selectivity index of 290 and 400 (HDAC6 and HDAC1, respectively). Recent investigations[14,15,31,32] have shown that eukaryotic parasites possess HDAC orthologues and that histone acetylation seems to play a key role in gene transcriptional regulation and cell cycle progression. Also, many human parasites share several characteristics with tumor cells, including high metabolic activity, a dependence on lactate fermentation as energy source within the human host, uncontrolled cell division, and a degree of invisibility to the host immune responses[14]. The therapeutic potential of HDAC inhibitors as anti-parasitic agents was first shown for the cyclic tetrapeptide apicidin[31]. In addition, several studies using various HDACi

demonstrated the anti-proliferative and anti-parasitic activity of these inhibitors on major human parasitic diseases such as leishmaniasis, malaria, schistosomiasis, toxoplasmosis, and trypanosomiasis[14,15].

So far, only class I (smHDAC1, smHDAC3 and smHDAC8) and class III (smSirt1, 2, 5, 6 and 7) HDACs of *S. mansoni* have been cloned and characterized[33,34]. Treatment of schistosomes with generic HDAC inhibitors caused protein acetylation and a dose-dependent mortality of schistosomula and adult worms[33]. All three *S. mansoni* class I HDACs (smHDAC1, 3 and 8) are expressed at all life-cycle stages, with HDAC8 transcripts being always the most abundant[32], indicating that this latter enzyme is a potential target for the design of schistosome specific inhibitors. This observation was quite surprising, because normal levels of HDAC8 transcripts are generally lower than those of HDAC1 and HDAC3 in human cells, with the exception of some cancers, where HDAC8 expression is often strikingly up-regulated[35].

The potential of smHDAC8 as a therapeutic target was supported by biochemical and *in vivo* assays[36]. RNA interference (RNAi)-mediated down-regulation of smHDAC8 expression in schistosome larvae, schistosomula, followed by their intravenous injection into mice and harvesting of the surviving worms 35 days later, showed a significantly reduced worm recovery compared to mice infected with schistosomula treated with control dsRNA[36]. Finally, the crucial roles of zinc-dependent HDACs in schistosome biology were confirmed with the use of small-molecule HDAC inhibitors[33,36,37]. Therefore, a therapy with small-molecule HDACi represents a promising approach for the treatment of schistosomiasis.

In a previous study, we were able to identify the first small molecule inhibitors of smHDAC8 by a combination of virtual screening and *in vitro* testing[38]. Two of the identified hits were co-crystallized with smHDAC8 paving the way for structure-based optimization[36]. Here,

we apply structure-based design on a benzohydroxamate template, taking into consideration appropriate synthetic strategies, to obtain compounds with smHDAC8 inhibitory activity *in vitro* and anti-schistosomal activity in cellular assays. A major goal of the current work was to identify compounds which show selectivity for smHDAC8 over major human HDAC isoforms, especially hHDAC1 and hHDAC6.

RESULTS AND DISCUSSION

STRUCTURAL VALIDATION

From the available X-ray structure of smHDAC8/**T5979345**[38] (Figure 1) it was known that an H-bond is formed between the amide-NH-group of the inhibitor and His292[38]. Therefore, open-ring analogs that maintained this hydrogen bond were designed. This resulted in the synthesis of the first series of inhibitors, 3-amino-benzohydroxamates **4a-4e** (Scheme 1) and 3-amido-benzohydroxamates **7a-7c**. (Scheme 2). The *in vitro* testing showed that all compounds show specificity for the HDAC8 isoforms over the other human HDACs tested (HDAC1 and 6). Yet, while the 3-amino-benzohydroxamates (**4a-e**) are micromolar inhibitors of both human and schistosomal HDAC8, they show a significant preference for the human isoform (Table 1). In contrast, the 3-amido-benzohydroxamates (**7a-c**) were active in the nanomolar range and showed a nearly similar inhibitory activity against hHDAC8 and smHDAC8. These results prompted us to focus on the derivatization of **7a-7c**, since this seemed to be a more promising strategy to obtain selective compounds.

However, prior to synthesis of derivatives of this series, we looked at the binding mode of this scaffold to smHDAC8. Towards this aim, the crystallographic structure at 2.3 Å of the complex between smHDAC8 and compound **7a** was solved and refined (Table S1 Supplementary Information). The crystal structure of the smHDAC8/**7a** complex reveals that the inhibitor binds in the smHDAC8 active site pocket, forming specific interactions with the protein (Figure 2). First and as expected, the hydroxamate warhead of **7a** interacts with both the catalytic zinc ion and three residues, namely His141, His142, and Tyr341 (Figure 2). The latter residue adopts the flipped-in conformation typically observed in most HDAC/hydroxamate complexes[11]. Second, reminiscent to what was observed in the

smHDAC8/**T5979345** complex[36], smHDAC8 H292 is able to interact with the inhibitor **7a**, its side chain forming a hydrogen bond (3.0 Å) with the amine group of the amide (Figures 2 and 3).

Strikingly, two additional smHDAC8-specific features were observed in this complex. First, and in contrast to what was observed for the smHDAC8/**T5979345** complex[36], smHDAC8 Phe151 is observed in its flipped-out position (Figures 2 and 3) despite the fact that binding of **7a** would not prevent the Phe151 side chain from adopting a flipped-in conformation. A major consequence of this flipped-out conformation of Phe151 is that Lys20 also adopts a flipped-in conformation, the aliphatic part of its side chain lying on the Phe151 side chain and its amine forming a hydrogen bond (2.8 Å) with the carbonyl oxygen of the **7a** amide group.

Interestingly, this is the first time that Lys20 has been observed interacting clearly with the inhibitor in a smHDAC8/inhibitor complex. Such a conformation had only been observed previously in the non-inhibited structure of smHDAC8 where Lys20 also interacted with an L-tartrate molecule that was present in the crystallization buffer and was observed binding to the catalytic zinc (Figure 3). In all other smHDAC8/inhibitor complexes solved so far, the Lys20 side chain was either not seen in density or was prevented from reaching into the active site by the flipped-in conformation adopted by Phe151[39].

In addition to these hydrogen bonds formed between smHDAC8 and **7a,** hydrophobic contacts between both molecules are also observed, building on the overall hydrophobic character of the smHDAC8 active site and further stabilizing the smHDAC8/**7a** interaction. Yet, the schistosome specific clamp formed by smHDAC8 Lys20 and His292, which distinctively interacts with the **7a** amide group, helps

anchoring **7a** in the enlarged – due to Phe151 flipping out – smHDAC8 active site, thus suggesting the molecular basis for the improved inhibitory activity of the 3-amido-benzohydroxamates towards smHDAC8.

SYNTHESIS

We then continued the optimization of the 3-amido-benzohydroxamate inhibitors. Towards this aim and to guide the optimization process, docking studies using the available inhibited hHDAC8 and smHDAC8 structures were carried out. Examination of the crystal structures showed that there is the possibility to use more bulky and more lipophilic residues at position 4 of the benzohydroxamate moiety. Recognizing that physicochemical properties might also play an important role for the anti-schistosomal activity, lipophilic substituents were also included. Taking this into consideration, we synthesized compounds **7d**–**j** containing different halides and alkoxy groups at position 4 to examine the effects of these substituents on the activity and selectivity for smHDAC8 (Scheme 2). The compounds containing halogen at position 4 of the benzohydroxamate moiety (**7d-f**) were slightly more selective for smHDAC8 compared to the 4-methoxy derivative **7c**. Compound **7h** with an ethoxy-group at position 4 did not show an increase in the activity against smHDAC8 but was less active on hHDAC8 compared to **7c**.

Meanwhile, the analogs containing more lipophilic alkoxy residues at position 4 such as **7i** and **7j** (Scheme 3) exhibited a decreased activity and selectivity for smHDAC8 compared to **7h**. Further modifications were introduced on the benzamide moiety including chloro, nitro or alkoxy groups (**7m**–**7p**, **7r**, **7t**, **7x**-**7z**). In addition, the introduction of aromatic lipophilic residues to address the hydrophobic side pocket of smHDAC8 (**7k**, **7l**, **7q**, **7u** – **7w**, **7za**) was investigated. Compound **7k** which has a quinolinyl residue and compound **7l** with a

4-biphenyl residue showed an increased activity against smHDAC8 and hHDAC8. A substitution in *meta*-position as in **7q** and *ortho*-position as in **7o** decreased the activity on the tested enzymes.

Interestingly, the combination of a *para*- and *ortho*-substitution as in **7p** could restore the activity against smHDAC8 without increasing the activity against the human enzymes. To prove that this substitution pattern is important for the selectivity of this compound, we synthesized compound **7z,** which was indeed found to be more active on the schistosomal enzyme than on the human counterpart. Increasing the distance between the two aromatic rings by a further methylene group (**7s)** led to increased smHDAC8 selectivity.

In addition, we tested further linker groups between the two aromatic rings (**9a, 10a,** Scheme 4). The introduction of an ether or sulfonamide resulted in a loss of activity for smHDAC8 and an increased activity for hHDAC8 compared to **7c**. Also, using other scaffolds like condensed aromatic ring systems in the case of **8a** did not result in an improvement of the activity or selectivity compared to **7c**.

To check the impact of the zinc chelating moiety we synthesized two analogs of **7l** containing a carboxylate and a carboxylester group instead of the hydroxamate (**11a** and **11b**, Scheme 5). As expected neither compound showed any effect in the enzymatic HDAC assay.

DOCKING STUDIES

To rationalize the obtained biochemical data, notably to understand the change of specificity between the schistosomal and human enzymes, the synthesized inhibitors were docked to the available crystal structures of smHDAC8, hHDAC8 and hHDAC1 and a homology model of hHDAC6. The applied docking method (for details see Methods section) was first successfully validated on the X-ray

structures of hHDAC8 and smHDAC8. Using this docking setup consistent binding models were derived for both human and smHDAC8 In the case of smHDAC8 all derivatives having an amide linker between the two aromatic rings showed hydrogen bonds to Lys20 and His292, as observed for **7a** in its crystal structure.

Most importantly, the hydrogen bond between the amide linker and His292 cannot be formed in hHDAC8 since His292 is replaced by a methionine in this latter enzyme. However, in the available crystal structures of hHDAC8 a conserved water molecule bound to the zinc coordinating histidine (His180 in hHDAC8) is observed which was found as a hydrogen bonding partner with most of the amides in the docking studies (Figure 4). Thus, the observed hydrogen bond in the case of hHDAC8 (as well as in the homology model of HDAC6) could partially explain the same range of activity of some of the compounds on human HDAC8 and HDAC6 isoforms as on smHDAC8.

Adding a substituent at the *para*-position of the parent compound **7a** (methyl, alkyloxy, and halide) results in a 2- to 7-fold gain in smHDAC8 inhibitory potency and a 2- to 20-fold gain in hHDAC8 potency, e.g. **7b**, **7c** and **7e** compared to **7a** (Table 1). Increasing the size of the substituent at the *para*-position enables additional interactions at the entrance of the pocket. Furthermore, the nature of the *para*-substituent might influence the biologically active conformation of the compounds, which affects not only the potency, but also the selectivity. In case of compound **7a** the X-ray structure shows an out-of-plane orientation of the amide linker (Φ: -60 to -102 degrees, Table S2 Supplementary Information) which is stabilized by two hydrogen bonds to Lys20 and His292 (Figure 2). A substituent at the *para*-position of the benzohydroxamate favors the out-of-plane conformation of the amide linker which might explain the higher inhibitory potency of the *para*-substituted compounds. Measuring the dihedral angle Φ between the amide linker and the first aromatic ring observed in the docking poses shows a clear preference for the out-of-plane conformation of the amide group (-77 to -90 degrees, Table

S2 Supplementary Information). In case of hHDAC8 the predicted conformation of the amide linker is close to a coplanar orientation (29 to 51 degrees, 148 degrees for **7g**) due to the modified hydrogen-bond pattern (Figure 4).

The decreased HDAC1 activity might be attributed to the narrower pocket of hHDAC1 in comparison to hHDAC8 and 6. In the docking poses, this can be clearly seen when comparing the distances between the zinc binding groups of *meta*-substituted benzohydroxamates to the zinc ion. In the case of hHDAC1, the distance is higher than in the other investigated HDAC isoforms (Figure 4). The docking results and SAR studies suggest that *meta*-substitution of benzohydroxamates is important to gain HDAC8 selectivity. This is also supported by previous publications, showing that *meta*-substituted benzohydroxamic acids are more active on human HDAC8 and HDAC6 in comparison to HDAC1 and other class I HDACs[28,30,40,41,42,43,44,45].

Adding hydrophobic substituents to the second aromatic ring such as halides or further aromatic rings (e.g. **7k**, **7l**, **7p**, **7z** and **7za**) resulted in additional van-der-Waals interaction with Phe216, Pro291 and Phe343 of smHDAC8. However, the higher selectivity of **7s** and **7z** (3-6 fold hHDAC8/smHDAC8 selectivity, 4-28 fold hHDAC6/smHDAC8 selectivity) could not be explained based on the derived docking solutions. More sophisticated methods taking into account protein flexibility and binding free energy calculations might be helpful to track down the subtle differences in the protein-ligand interactions deep inside the binding pocket.

PHENOTYPIC RESPONSE

We next analyzed the effect of the developed compounds on the parasites maintained in culture. The compounds were initially tested for their toxicity toward *S. mansoni* schistosomula using an AlamarBlue-based viability assay (see Experimental Methods). Initial testing was

done at a concentration of 10 µM and selected compounds were also tested at 20 µM in order to determine dose-dependency. Two biological replicates were carried out in triplicate and the results are shown in Table 2. In addition to the compounds developed during this study, the selective HDAC8 inhibitor **PCI-34051** and the praziquantel, the drug used for treating schistosomiasis, were also included in the assay. Of the tested compounds, **7l** and **7za** provoked the most marked dose-dependent reductions in schistosomula viability. In this assay **PCI-34051** showed only very modest activity against schistosomula and praziquantel was inactive at the concentrations used. This latter result is in line with previous findings[46] and this was thought to be due in part to the relatively weak activity of praziquantel on schistosomula and to a stimulation of enzyme or ion channel activity, leading to high fluorescence signals in the assay. In view of its selectivity of inhibition with regard to human HDAC1 and 6, inhibitor **7l** was chosen for further testing. We first showed that the EC_{50} value for this compound using the AlamarBlue-based assay was 16.1 µM (Figure S1, Supplementary Information). We next showed that compound **7l** was lethal for schistosomula in a microscopy-based assay within 2 days of incubation at 10 µM and 1-2 days at 20 µM (Figure 5A, 5B). We further tested derivatives of **7l** that were synthesized (**11a** and **11b**, Scheme 5) as negative controls to check **7l** for off target effects. In the same assay the compound **11a**, an analogue of **7l** (carboxyester instead of hydroxamate) with no inhibitory activity on smHDAC8, had only a very minor effect on schistosomula after 5 days of incubation compared to the solvent (DMSO) control (Figure 5A, 5B). This suggested that the activity of **7l** on schistosomula was indeed related to its capacity to inhibit smHDAC8. We finally tested compound **7l** for its capacity to affect adult schistosomes maintained in culture (Figure 5C, 5D). Concentrations of 10 and 20 µM of **7l** caused a marked separation of adult male and female worm pairs, 90% of the pairs being separated after 5 days in the presence of 20 µM **7l**. A corresponding reduction in egg laying by these worm pairs was also induced (Figure 5D), of 80% for the 20 µM

dose. Therefore, compound **7l** affects the viability of both larvae and adult worms of *S. mansoni*, most probably through the inhibition of smHDAC8.

CYTOTOXICITY ASSAY

It was important to test the selectivity of the compounds against smHDAC8 and to exclude possible toxic effects caused by targeting human HDACs or other proteins. Therefore, a cytotoxicity assay in a human epithelial kidney cell line (HEK293) was performed. The cells were incubated for 45 hours with the indicated compounds in a concentration of 50 µM and the cell viability was determined by using the AlamarBlue-assay. All tested inhibitors exhibited only a relatively low cytotoxicity in the human cell system used (Table 3).

CONCLUSIONS

Our initial work on HDAC8 from *Schistosoma mansoni* has provided the proof of concept that HDAC inhibitors of this enzyme could be used for targeting pathogens[36]. Here, a weak screening hit with suboptimal physicochemical properties characterized from this initial study was optimized against HDAC8 from *S. mansoni* using critical structure-guided insights. Central to this optimization was the inclusion of a methyl/methoxy-group in the *para*-position and an amide linker in the *meta*-position of the benzohydroxamate. Previous crystallographic studies highlighted the binding of the inhibitors at the acetyl-lysine tunnel and featured a flexible phenylalanine that was able to shift in response to compound binding to smHDAC8. The series disclosed here builds on this initial structural feature and represents a novel smHDAC8 inhibition template which gives the possibility to develop potent and selective inhibitors for the therapy of

schistosomiasis. The presented compounds demonstrated high selectivity for smHDAC8 over the major human HDAC isoforms HDAC1 and HDAC6, and some compounds even showed a preference for smHDAC8 over its human ortholog hHDAC8. It has been reported that inhibition of human HDAC8 shows limited effects on many cell types[39] and that an HDAC8 inhibitor had the most limited effect on the human acetylome among a panel of inhibitors of HDACs with different selectivites[47]. Cytotoxicity studies of the tested compounds showed that the compounds present a relatively low effect on cell proliferation indicating that the inhibition of human HDAC8 does not result in an intrinsic toxicity. Thus, while we recognize that selectivity over human HDAC8 still needs optimization, there are strong indications that the high selectivity with respect to hHDAC1 and 6 that we have already obtained is more important for a potential therapeutic setting. The most potent derivatives were also shown to impair the viability of schistosomula without affecting cell viability of HEK293 cells. One such compound, **7l**, killed schistosomula in vitro, caused significant separation of adult worm pairs and a significant decrease in egg laying. An analog of **7l**, without inhibitory activity toward smHDAC8, had no effect on the parasite, confirming that inhibition of smHDAC8 is the basis of the anti-parasitic effects of these inhibitors and underlining their potential as anti-schistosomal drug leads.

EXPERIMENTAL METHODS

SYNTHETIC CHEMISTRY

Unsubstituted and 4-substituted 3-amino benzoic acids were used as starting points for the synthesis of the inhibitors under study. Alkyl and aryl residues were introduced at the aromatic-NH_2 group via reductive amination of the imine, obtained by the reaction of the amino group of the 3-amino-benzoic acids and an aldehyde using sodium triacetoxy borohydride as reducing reagent. To avoid by-products in the following synthetic steps, the secondary amine was protected by *tert*-butyloxycarbonyl(Boc) group. The corresponding hydroxamates (**4a-e**) were obtained using PyBOP as activating reagent and *O*-(tetrahydro-2*H*-pyran-2-yl)hydroxylamine and the subsequent cleavage of the protecting groups (Scheme 1). The 4-amido-benzohydroxamate derivatives (**7a-g, 7k-z**) were prepared from different 3-amino-benzoic acids with modifications in position 4 and various benzoic acid derivatives (**8a-10a**). The conversion of the amino group to the corresponding amide was accomplished by the reaction with activated benzoic acid derivatives and DIPEA. Different methods for the activation of the carboxylic acids were tested. PyBOP, DCC and chloro ethyl formiate were insufficient and byproducts were produced, so the activation with thionylchloride was selected as the method of choice. Using 3-amino-methyl-benzoate derivatives instead of 3-amino-benzoic acid derivatives increased the yields and also facilitated the purification. The corresponding hydroxamates were obtained using PyBOP and *O*-(tetrahydro-2*H*-pyran-2-yl)hydroxylamine followed by cleavage of the protecting group (Scheme 2). Generally, using THP-protected hydroxylamine increased the yields of the desired benzohydroxamates compared to other methods using hydroxylamine hydrochloride and KOH or potassium methanolate.

Several inhibitors could be synthesized directly from commercially available carboxylic acids (**8a-10a**) (Scheme 3). In other cases, the inhibitors were synthesized starting from 4-alkoxy-benzoic acid derivatives and a following nitration step (**7h-j, 7za**) (Scheme 4). For the nitration step nitrating acid, which is a mixture of 1 ml nitric acid (68%) and 1.2 ml sulfuric acid (98%), was used. This method is suitable for the reaction of 10 mmol moderately activated aromatic rings. After the purification step the nitro-group was reduced to the corresponding amine-group via Fe^0 and dil. hydrochloric acid.

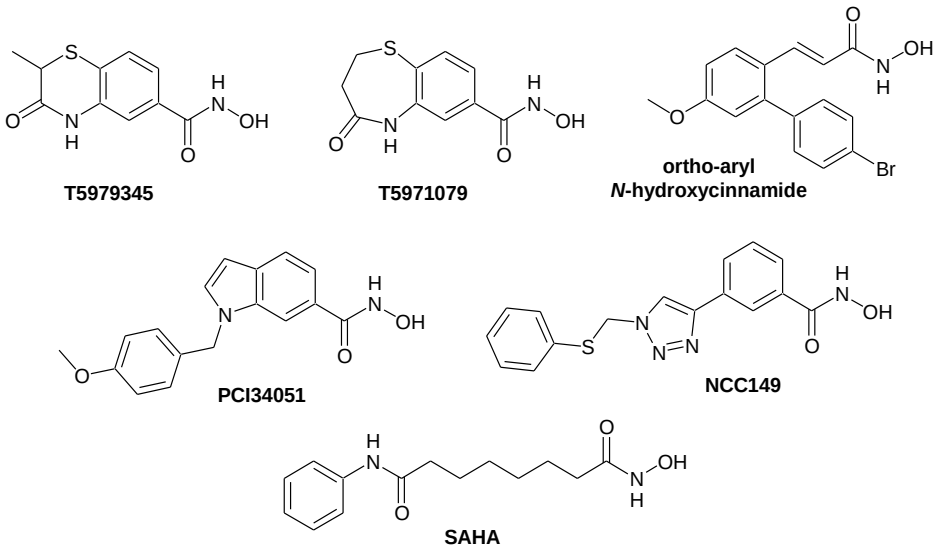

Figure 1. Chemical structures of the pan-HDAC inhibitor SAHA and reported hHDAC8 inhibitors.

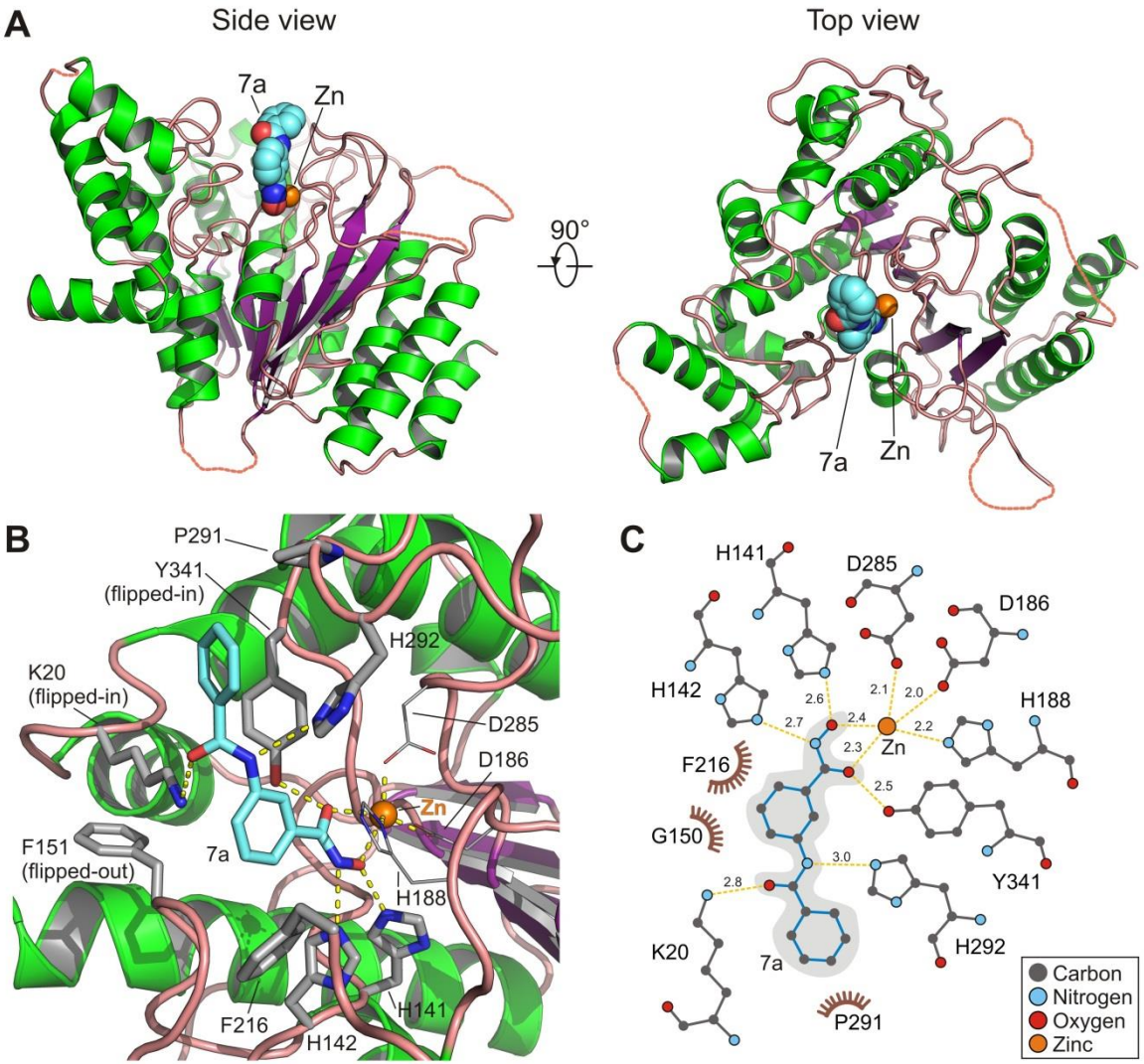

Figure 2. Overall structure of inhibitor **7a** bound to smHDAC8.

(**A**) Ribbon representation of the structure of smHDAC8 with bound **7a** represented in space-filling; the orange sphere represents the catalytic zinc ion.

(**B**) Close-up view of the binding mode of **7a** in the smHDAC8 active site pocket. Protein residues are shown as grey sticks and **7a** as cyan sticks. Yellow broken lines represent salt bridges made by smHDAC8, **7a** and the catalytic zinc ion.

(**C**) LigPlot-generated two-dimensional schematic overview of molecular interactions between **7a** and smHDAC8 active site zinc and protein residues. Hydrogen bonds and interactions are indicated by yellow dashed lines with corresponding distances between the atoms given in Å. Hydrophobic contacts are shown by brown arcs with spokes radiating toward the atoms involved.

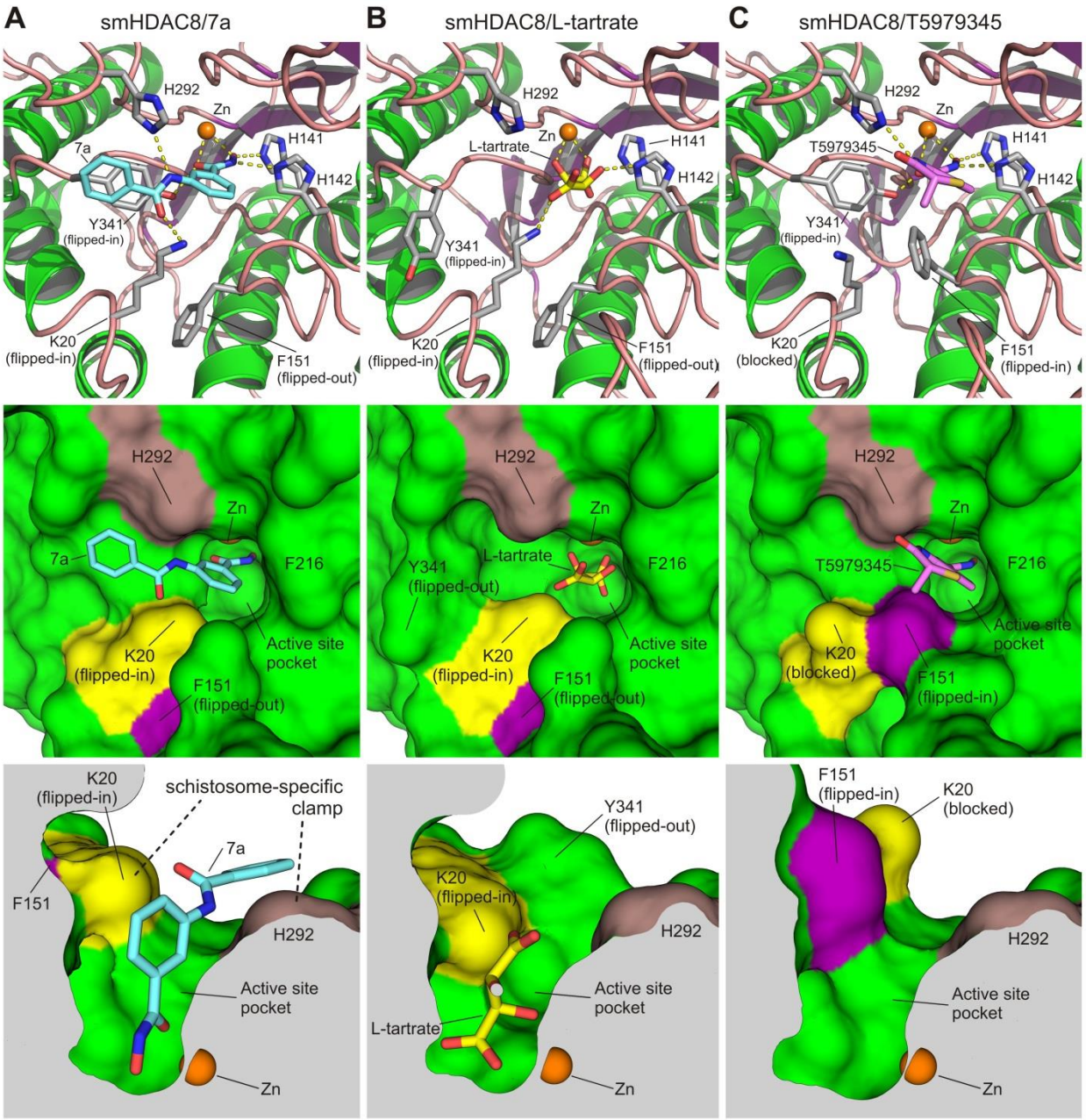
A
smHDAC8/7a
B
smHDAC8/L-tartrate
C
smHDAC8/T5979345
H292
Zn
H141
H142
7a
L-tartrate
T5979345
Y341
(flipped-in)
K20
(flipped-in)
F151
(flipped-out)
K20
(blocked)
F151
(flipped-in)
F216
Active site
pocket
Y341
(flipped-out)
schistosome-specific
clamp

Figure 3. Specific structural interactions observed in the smHDAC8 active site pocket with bound inhibitor **7a**. Upper panels, close-up views with protein and small molecules shown as ribbon and sticks; Middle panels, surface representations; Lower panels, cut-away surface representations of the active site of the (A) smHDAC8/**7a** complex, (B) smHDAC8/L-tartrate complex, and (C) smHDAC8/**T5979345** complex. Note that for clarity the **T5979345** molecule was removed from the cut-away surface representation picture in (C). In the smHDAC8/**7a** complex structure in (A), specific structural arrangements are observed, notably involving two specific residues: Lys20 and Phe151. The flipped-out conformation of Phe151 enables Lys20 to flip-in and to contact inhibitor **7a**. This unique active site conformation is not observed in other smHDAC8/inhibitor complexes. In addition, the schistosome-specific residue His292 together with the flipped-in Lys20 form a clamp that promotes stabilization and binding of **7a** in the smHDAC8 active site pocket.

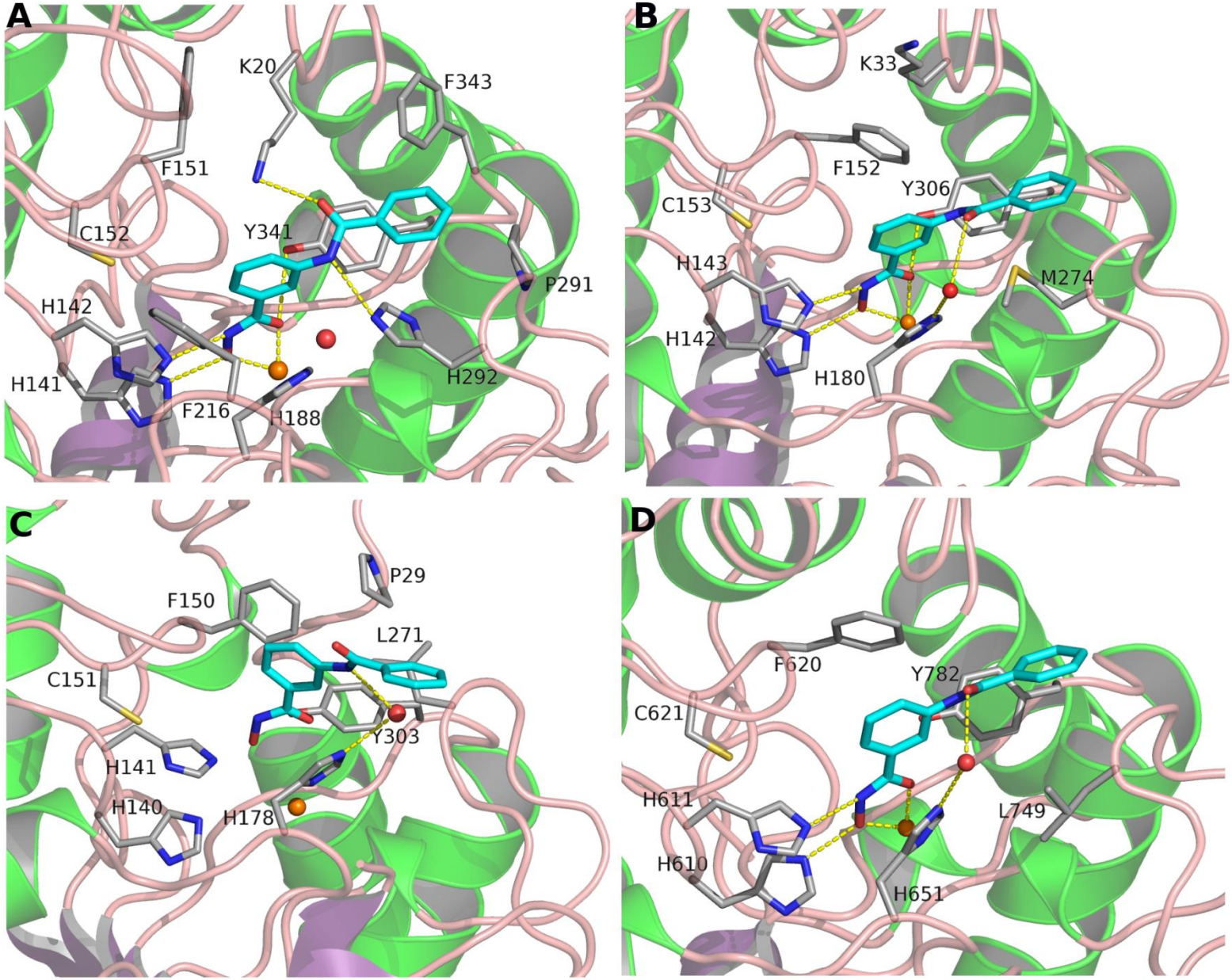
A
K20
F343
F151
C152
Y341
P291
H142
H141
H292
F216
H188
B
K33
F152
Y306
C153
H143
M274
H142
H180
C
P29
F150
L271
C151
Y303
H141
H140
H178
D
F620
Y782
C621
H611
L749
H610
H651

Figure 4. Docking poses of compound **7a** (cyan carbon atoms) in the X-ray structure of (a) smHDAC8 (this study), (b) hHDAC8 (PDB ID 2V5X), (c) hHDAC1 (PDB ID 5BKX) and (d) homology model of hHDAC6. The protein backbone is depicted in ribbon representation and the side chains of important residues in stick representation with carbons colored grey. The conserved water molecule that should help stabilize **7a** binding in the active sites of hHDAC6 and hHDAC8 is shown as a red ball, and the zinc ion as an orange ball. Hydrogen bonds and interactions with the metal ion are depicted as yellow dashed lines.

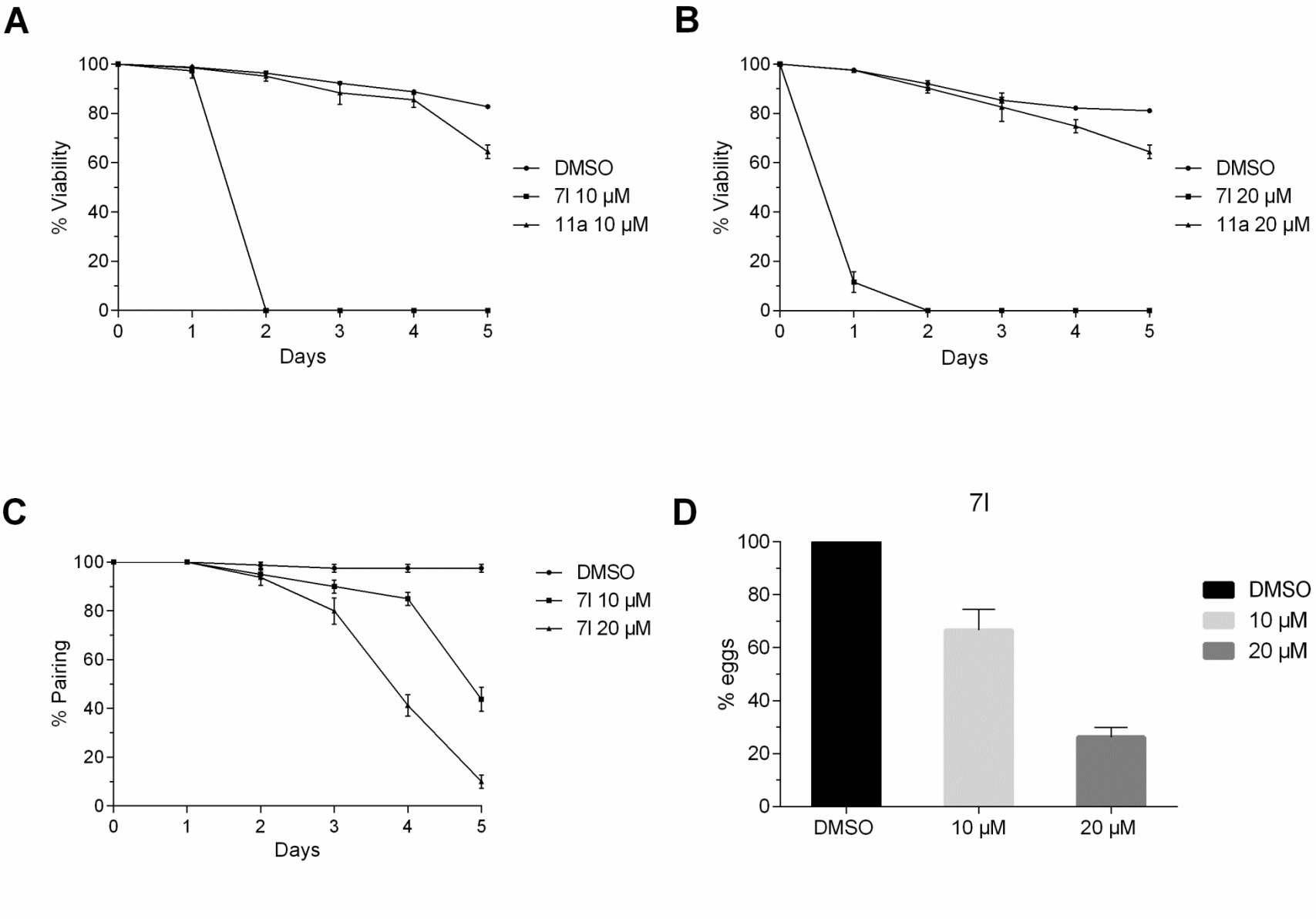
A
% Viability
Days
DMSO
7l 10 µM
11a 10 µM
B
% Viability
Days
DMSO
7l 20 µM
11a 20 µM
C
% Pairing
Days
DMSO
7l 10 µM
7l 20 µM
D
7l
% eggs
DMSO
10 µM
20 µM

Figure 5. A) Viability assay of *S. mansoni* schistosomula with up to 5 days of incubation with 10 µM **7l** or **11a** compared to the solvent (DMSO) control. **B)** The same assay with 20 µM **7l** or **11a**. **C)** Separation of adult worm pairs for up to 5 days in culture in the presence of 10 or 20 µM 7l. **D)** Cumulative reduction (%) in egg laying by adult worm pairs in culture in the presence of 10 or 20 µM **7l** compared to the solvent (DMSO) control.

Scheme 1.

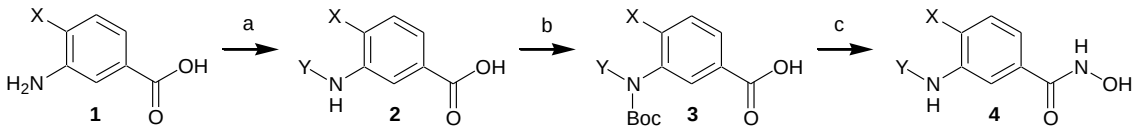

4a: X = H; Y = benzyl
4b: X = H; Y = cyclohexyl
4c: X = H; Y = *N,N*-dimethyl
4d: X = H; Y = *N,N*-dibenzyl
4e: X = methyl, Y = cyclohexyl

(a) aldehyde, toluene, $Na(AcO)_3BH$, AcOH; (b) Boc_2O, MeOH, *t*-BuOH; (c) PyBOP, DIPEA, NH_2OTHP, THF; cat. HCl, THF; TFA, $CHCl_3$

Scheme 2.

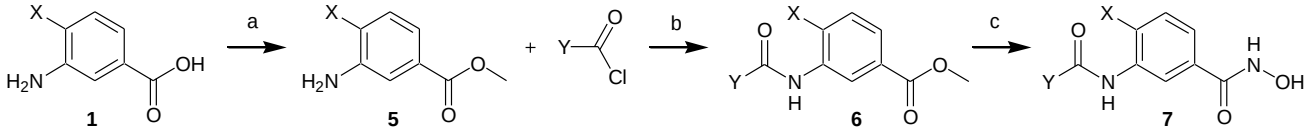

7a: X = H; Y = phenyl
7b: X = methyl; Y = phenyl
7c: X = methoxy; Y = phenyl
7d: X = fluoro; Y = phenyl
7e: X = chloro; Y = phenyl
7f: X = bromo; Y = phenyl
7g: X = trifluormethyl; Y = phenyl

7h: X = ethoxy; Y = phenyl
7i: X = propoxy; Y = phenyl
7j: X = isopropoxy; Y = phenyl
7k: X = methyl; Y = quinolinyl
7l: X = methoxy; Y = 4-biphenyl
7m: X = methoxy; Y = 4-methoxyphenyl
7n: X = methoxy; Y = 4-chlorophenyl

7o: X = methoxy; Y = 2-chlorophenyl
7p: X = methoxy; Y = 2,4-dichlorophenyl
7q: X = methoxy; Y = 3-biphenyl
7r: X = methoxy; Y = 4-ethoxyphenyl
7s: X = methoxy; Y = benzyl
7t: X = chloro; Y = 4-methoxyphenyl
7u: = chloro; Y = 3-benzyloxyphenyl

7v: X = chloro; Y = 3-phenoxyphenyl
7w: X = chloro; Y = 4-phenoxyphenyl
7x: X = chloro; Y = 4-chlorophenyl
7y: X = chloro; Y = 4-nitrophenyl
7z: X = chloro; Y = 2,4-dichlorophenyl
7za: X = ethoxy; Y = 4-biphenyl

(a) $SOCl_2$, MeOH; (b) DIPEA, THF; (c) aq. NaOH sol., MeOH; PyBOP, DIPEA, NH_2OTHP, THF; cat. HCl, THF

Scheme 3.

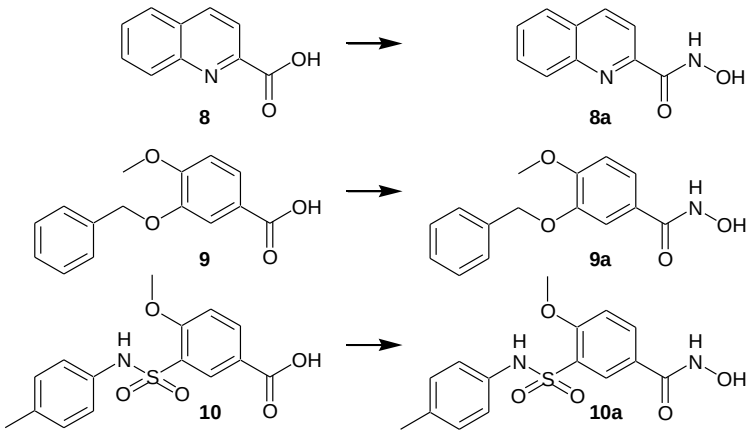

PyBOP, DIPEA, NH_2OTHP, THF; cat. HCl, THF

Scheme 4.

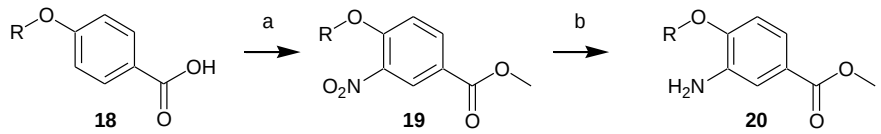

R: **20a**) CH_3-CH_2-; **20b**) CH_3-$(CH_2)_2$-; **20c**) $(CH_3)_2$-CH-

(a) HNO_3/H_2SO_4; (b) Fe^0, dil. HCl, MeOH

Scheme 5.

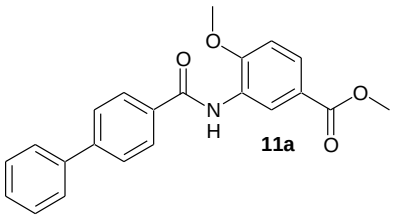

11a

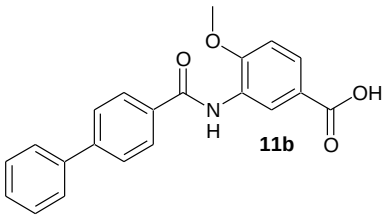

11b

Table 1: IC_{50}-values for 3-Amino-benzohydroxamate derivatives.

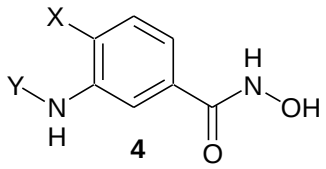

4

Cpd. no.	X	Y	smHDAC8 IC_{50} nM	hHDAC8 IC_{50} nM	hHDAC1 IC_{50} µM	hHDAC6 IC_{50} µM
4a	H	benzyl	1080 ± 250	143.4 ± 7.3	41.4% @ 10µM	n.d.
4b	H	cyclohexyl	3630 ± 620	830 ± 40	129.9 ± 18.5	n.d.
4c	H	*N*,*N*-dimethyl	1576 ± 146.0	70.2 ± 10.8	37.4% @ 10µM	n.d.
4d	H	*N*,*N*-dibenzyl	9290 ± 1500	2190 ± 420	42.3 ± 3.8	8.6 ± 1.9
4e	methyl	cyclohexyl	600.3 ± 195.5	104.3 ± 12.0	49.5% @ 10µM	n.d.

Table 1 (continued): IC_{50}-values for the 3-Amido-benzohydroxamate derivatives.

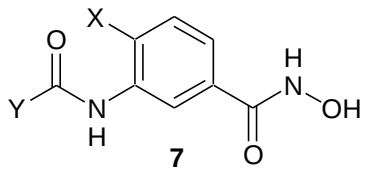

7

Cpd. no.	X	Y	smHDAC8 IC_{50} nM	hHDAC8 IC_{50} nM	hHDAC1 IC_{50} µM	hHDAC6 IC_{50} µM
7a	H	phenyl	468.2 ± 79.0	582.0 ± 48.0	33.6 ± 1.8	3.0 ± 0.3
7b	methyl	phenyl	116.2 ± 38.2	204.0 ± 22.0	8.4 ± 2.0	0.9 ± 0.4
7c	methoxy	phenyl	189.8 ± 54.2	88.3 ± 24.0	2.3 ± 1.2	2.5 ± 1.1
7d	fluoro	phenyl	177.6 ± 8.1	317.8 ± 54.2	22.3 ± 7.7	0.50 ± 0.01
7e	chloro	phenyl	67.0 ± 10.2	120.0 ± 36.7	11.6 ± 3.9	0.12 ± 0.02
7f	bromo	phenyl	150.4 ± 8.5	191.4 ± 26.0	7.4 ± 0.8	0.15 ± 0.01
7g	trifluoro-methyl	phenyl	139.6 ± 8.3	342.2 ± 76.1	2.4 ± 0.1	0.14 ± 0.02
7h	ethoxy	phenyl	129.3 ± 7.6	171.5 ± 15.6	4.6 ± 0.3	1.3 ± 0.1
7i	propoxy	phenyl	266.9 ± 49.5	n.d.	n.d.	n.d.
7j	isopropoxy	phenyl	220.1 ± 56.2	29.0 ± 0.2	3.6 ± 0.3	2.6 ± 0.4

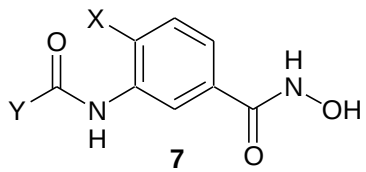

7

Cpd. no.	X	Y	smHDAC8 IC_{50} nM	hHDAC8 IC_{50} nM	hHDAC1 IC_{50} µM	hHDAC6 IC_{50} µM
7k	methyl	2-quinaldin	96.1 ± 13.7	30.3 ± 7.3	2.7 ± 0.8	0.09 ± 0.01
7l	methoxy	4-biphenyl	75.4 ± 25.5	26.1 ± 17.6	6.3 ± 2.1	0.390 ± 0.002
7m	methoxy	4-methoxy-phenyl	106.0 ± 17.5	77.1 ± 10.6	2.6 ± 0.2	0.4 ± 0.1
7n	methoxy	4-chloro-phenyl	146.0 ± 4.3	239.7 ± 96.0	2.9 ± 0.3	0.9 ± 0.1
7o	methoxy	2-chloro-phenyl	699.3 ± 27.4	211.16 ± 27.59	9.6 ± 1.0	3.1 ± 0.7
7p	methoxy	2,4-dichloro-phenyl	121.6 ± 18.7	548.3 ± 93.9	13.0 ± 1.9	2.3 ± 0.4
7q	methoxy	3-biphenyl	289.7 ± 20.0	n.d.	n.d.	n.d.
7r	methoxy	4-ethoxyphenyl	305.0 ± 35.0	438.4 ± 48.0	4.4 ± 0.6	1.0 ± 0.1
7s	methoxy	benzyl	182.7 ± 39.3	512.2 ± 29.8	28.9 ± 8.6	5.1 ± 0.7
7t	chloro	4-methoxy-phenyl	147.1 ± 4.8	235.6 ± 49.5	4.1 ± 0.9	0.13 ± 0.01
7u	chloro	3-benzyloxy-phenyl	378.1 ± 44.9	214.4 ± 27.0	9.4 ± 2.8	1.5 ± 0.1

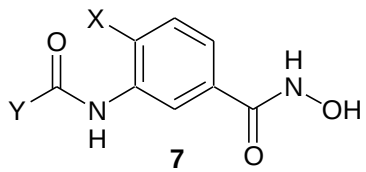

7

Cpd. no.	X	Y	smHDAC8 IC_{50} nM	hHDAC8 IC_{50} nM	hHDAC1 IC_{50} µM	hHDAC6 IC_{50} µM
7v	chloro	3-phenoxy-phenyl	396.4 ± 43.3	448.6 ± 100.4	6.4 ± 0.7	0.3 ± 0.1
7w	chloro	4-phenoxy-phenyl	979.1 ± 1100	1080 ± 300	8.5 ± 2.1	0.15 ± 0.01
7x	chloro	4-chloro-phenyl	234.7 ± 10.3	292.0 ± 53.3	3.8 ± 0.2	0.09 ± 0.05
7y	chloro	4-nitro-phenyl	393.6 ± 50.5	n.d.	n.d.	n.d.
7z	chloro	2,4-dichloro-phenyl	191.4 ± 16.7	1184.0± 45.1	31.6 ± 19.8	0.8 ± 0.1
7za	ethoxy	4-biphenyl	92.0 ± 26.0	148.7 ± 22.7	2.08 ± 0.14	0.6 ± 0.1
8a			8205 ± 1300	582.3 ± 88.5	n.d.	n.d.
9a			268.2 ± 21.1	23.9 ± 4.7	12.1 ± 5.7	2.9 ± 0.3
10a			485.0 ± 158.2	19.8 ± 5.9	20.0 ± 5.9	2.4 ± 0.9
11a			n.a.	n.a.	n.a.	n.a.
11b			n.a.	n.a.	n.a.	n.a.
T5979345			1480 ± 460	970 ± 110	27.5 ± 8.3µM	3.6 ± 0.6µM
T5971079			1220 ± 280	620 ± 80	9.8 ± 0.7µM	1.3 ± 0.2µM
PCI34051			435.6 ± 61.0	77.7 ± 28.1	48% @ 100µM	41% @ 100µM

SAHA	1560 ± 200	400 ± 100	0.117 ± 0.006	0.042 ± 0.011

Table 2. Toxicity studies on *S. mansoni* schistosomula (AlamarBlue assay).

Cpd.	10 µM		20 µM	
no.	% viability	± SEM	% viability	± SEM
4b	82.7	2.4	n.d.	n.d.
4c	92.6	7.4	n.d.	n.d.
4d	77.9	2.6	74.6	0.4
4e	84.3	1.7	n.d.	n.d.
7a	79.2	0.5	75.6	5.1
7b	82.9	2.0	72.4	2.4
7c	77.4	3.2	74.8	2.3
7d	82.0	8.1	78.6	9.5
7e	84.7	1.4	n.d.	n.d.
7f	70.8	4.4	63.1	1.7
7g	99.9	0.8	77.4	3.4
7h	89.7	10.3	n.d.	n.d.
7j	75.0	0.8	68.7	0.7
7k	74.9	4.1	59.4	4.2

7l	64.8	3.5	33.4	3.5
7m	74.6	6.7	64.6	1.0
7o	89.5	7.2	66.5	0.8
7p	77.8	2.4	50.7	2.7
7q	58.8	1.6	57.0	1.2
7s	83.3	4.2	82.8	5.8
7t	63.2	0.5	60.7	0.3
7u	73.8	5.4	68.6	2.4
7v	62.9	2.7	55.0	3.9
7x	71.8	4.1	49.3	0.6
7y	85.3	6.8	68.1	1.2
7z	72.5	0.3	59.3	9.9
7za	77.9	3.9	35.8	0.8
8a	95.6	4.4	n.d.	n.d.
10a	77.7	5.0	73.8	4.2
PCI-34051	70.6	0.5	62.3	3.5
Praziquantel	92.0	7.5	89.0	5.7

Table 3. Cytotoxicity studies in HEK293 cells.

Cpd. no.	Viability* (%)	Cpd. no.	Viability* (%)	Cpd. no.	Viability* (%)
4a	n.d.	7**h**	70.4	**7t**	62.5
4b	70.7	**7i**	97.4	**7u**	74.4
4c	92.7	**7**j	128.6	**7v**	62.0
4d	7.7	**7k**	66.2	**7w**	n.d.
4e	70.2	**7l**	12.3 (199 µM)$^{+}$	**7x**	81.6
7a	72.0	**7m**	61.9	**7y**	79.1
7b	71.2	**7n**	92.6	**7z**	70.4
7c	67.3	**7o**	96.9	**7za**	80.3
7d	81.8	**7p**	95.1	**8a**	73.3
7e	72.2	**7q**	76.2	**9a**	69.1
7f	64.3	**7r**	87.7	**10a**	80.2
7g	96.0	**7s**	88.7	**11a**	47.2

7h	70.4	**7t**	62.5	**11b**	86.9

* Viability of cells in presence of 50 µM compound in comparison to an untreated sample. As positive control daunorubicin was used and an IC_{50} value of 12.55 ± 0.07 µM was determined.

$^{+}IC_{50}$ value,

n.d. not determined

Materials

All materials and reagents were purchased from Sigma–Aldrich Co. Ltd. and Carbolution Chemicals. All solvents were analytically pure and dried before use. Thin layer chromatography was carried out on aluminum sheets coated with silica gel 60 F254 (Merck, Darmstadt, Germany). For column chromatography under normal pressure silica gel 60 (0.036–0.200mm) was used.

Final compounds were confirmed to be of >95% purity based on HPLC. Purity was measured by UV absorbance at 256 nm. The HPLC consists of an XTerra RP18 column (3.5 µm 3.9 x 100 mm) from the manufacturer Waters (Milford, MA, USA) two LC-10AD pump, a SPD-M10A VP PDA detector, and a SIL-HT auto sampler all from the manufacturer Shimadzu (Kyoto, Japan). The mobile phase was in all cases a gradient of methanol/water (starting at 95% water going to 5% water).

Mass spectrometry analyses were performed with a Finnigan MAT 710C (Thermo separation Products, San Jose, USA) for the ESI-MS spectra, and with a LTQ (linear ion trap)-Orbitrap XL hybrid mass spectrometer (Thermo Fisher Scientific, Bremen, Germany) for the HRMS-ESI (high resolution mass spectrometry) spectra. For the HRMS analyses the signal for the isotopes with the highest prevalence was given and calculated (^{35}Clor, ^{79}Brom).

^{1}H NMR and ^{13}C NMR spectra were taken on a Varian Gemini 2000 and a Varian Inova 500 using deuterated chloroform ($CDCl_3$) and deuterated DMSO ($(CD_3)_2SO$) as solvent. Chemical shifts are referenced to the residual solvent signals. The following abbreviations for solvents and reagents were used: ethyl acetate (EtOAc), methanol (MeOH), tetrahydrofuran (THF), chloroform ($CHCl_3$), water (H_2O).

Computational studies

Homology modeling of hHDAC6 was performed using the program MODELLER[48] as described in a previous publication[38]. Molecular docking of all inhibitors to X-ray structures of smHDAC8, hHDAC8, hHDAC1 and the homology model of hHDAC6 was carried out using the progam Glide[49] (Schrödinger, LLC, New York, NY, USA). The same protocol was used as in a previous study[37]. Briefly, the protein structures were prepared using Schrödinger's Protein Preparation Wizard. Hydrogen atoms were added, protonation states were assigned and a restrained minimization was performed. Inhibitor structures were prepared in MOE 2012.10 (Chemical Computing Group, Montreal, Canada). All compounds were docked in neutral form with multiple low energy starting conformations to produce more unbiased results.

Enzymes and *in vitro* inhibition assays

Recombinant human HDAC1 and 6 were purchased from BPS biosciences, and recombinant human HDAC8 was produced as described before[36]. Recombinant smHDAC8 enzyme was overproduced in *E. coli* cells and purified by a method previously described[36]. Inhibition assays of smHDAC8 and human HDACs were performed as described earlier[36,37]. Briefly, the commercial Fluor de Lys drug discovery kit ((BML-KI178) was used for testing inhibition of smHDAC8 and human HDAC8. Test compounds, Fluor de Lys-HDAC8 substrate (50 µM) and enzyme were incubated for 90 minutes at 37°C with subsequent addition of 50 µL Developer II (BML-KI176) and further incubation for 45 minutes at 30°C. Fluorescence was measured in a plate reader (BMG Polarstar) with excitation at λ = 390 nm and emission at λ = 460 nm. Inhibition tests of human HDAC1 and 6 were conducted using ZMAL (Cbz-(Ac)Lys-AMC) as substrate and trypsin as a developer. After incubation of test compounds, ZMAL (10.5 µM) and enzyme for 90 minutes at 37°C, 60 µL of trypsin was

added and further incubated for 20 minutes at 37°C. Trichostatin A (2 µM) was used in both assays to stop the reaction. Fluorescence was measured similarly as mentioned above. IC_{50} values were determined with OriginPro (version 9.0.0, Northampton, Massachusetts). Values in Table 1 represent mean ± S.E.

Cytotoxicity studies

HEK293 cells (DSMZ Braunschweig, ACC305) were incubated at 37°C in a humidified incubator with 5% CO_2 in Dulbecco's Modified Eagle Medium (DMEM) supplemented with 10% FCS and 5 mM glutamine. Cells were seeded out at 1.5 x 10^3 cells per well in a 96-well cell culture plate (TPP, Switzerland). The compounds were added immediately to the medium at 50 µM or increasing concentrations to determine IC_{50} values. After 24 h AlamarBlue reagent (Invitrogen, CA) was added according to the manufacturer's instructions and incubated again for 21 h before samples were analysed. Detection of viable cells which convert the resazurine compound of reagent into the high fluorescent resorufin was performed by using a FLUOstarOPTIMA microplate reader (BMG Labtec) with the following filter set: Ex 560 nm / Em 590 nm. All measurements were performed in triplicates and data are means with SD $\leq$ 12%. As a positive control daunorubicin was used and an IC_{50} value of 12.55 ± 0.07 µM was determined.

Phenotypic screening

The screening assay to determine the effects of novel inhibitors targeting smHDAC8 on the viability of *S. mansoni* schistosomula was carried out as previously described[50]. Briefly, newly transformed schistosomula (NTS) were obtained *in vitro* by mechanical

transformation of *S. mansoni* cercaria as previously described[51]. An NTS suspension was prepared at a concentration of 100 NTS per 100 µL using Medium 199 (Invitrogen) supplemented with 10% fetal calf serum (Gibco), penicillin (50 $U.mL^{-1}$), streptomycin (50 $\mu g.mL^{-1}$) and rifampicin (60 $\mu g.mL^{-1}$). Schistosomula were kept in culture 3 hours at 37°C and 5% CO_2 prior to use in screening. Drug stock solutions of 20 mM in DMSO were used. Mid-dilutions were performed in 100% DMSO and 1 µl added to 100 µl/well of M199 medium in black 96 well plates (Nunc, UK) with supplemented Medium 199 and 100 µl of prepared NTS suspension (100 NTS/well). Live and dead schistosomula (treated with 70% ethanol) were use as positive and negative controls. Experiments were carried out in triplicate wells in two biological replicates and the compounds were tested at final concentrations of 10 and 20 µM. After 48 hours of drug exposure 20 µL of resazurine solution (AbdSerotec) were add in each well. Finally, after a further 24 hours of exposure, the fluorescence intensity of the highly red fluorescent resorufin product was measured using at an excitation wavelength of 530 nm and an emission wavelength of 590 nm in an Infinite M200 Pro microplate reader (TECAN). Background fluorescence of the drug containing medium was determined for each drug dilution using wells containing only DMSO as control. The EC_{50} concentration for compound **7l** was measured using the same assay with different concentrations of the compound.

The effect of selected compounds on the viability of schistosomula was further tested using a microscopy based assay as described. Schistosomula (2,000 per well), prepared as described above, were maintained in 6-well plates in M199 medium kept at pH 7.4 with 10 mM HEPES and supplemented as above at 37°C in a humid atmosphere containing 5% CO_2. Two different concentrations of inhibitors (10 and 20 µM) were added, dissolved in DMSO, and the culture medium was refreshed each day. The assessment of parasite mortality was carried out after microscopic examination, based on three criteria: a granular appearance, tegumental defects and the absence of

motility. At least 300 schistosomula were observed at each time point for each condition and results were expressed as a percentage of viable larvae remaining. Three biological replicates (different batches of larvae) were examined in duplicate for each condition.

The stability of adult worm pairs and egg laying was assayed as previously described[51]. Worm pairs were obtained from infected hamsters by perfusion as described[53], washed in M199 medium and ten pairs placed in 2 mL of M199 buffered complete medium (as for schistosomula above) in each well of a 6-well culture plate. Worms were maintained in culture for 5 days at 37°C (humid atmosphere, 5% CO_2) before the addition of smHDAC8 inhibitors dissolved in DMSO as above. Both the culture medium and the inhibitors were refreshed daily. The number of couples remaining as pairs was determined daily by microscopy and the medium of each well containing eggs laid by the couples was recovered and centrifuged to allow eggs to be counted under the microscope. Two biological replicate experiments were performed in triplicate.

Crystallization and X-ray data collection

Diffraction-quality crystals of native smHDAC8 enzyme were obtained at 17°C after three to four days by mixing equal volumes of smHDAC8 (2.5 mg/ml) with reservoir solution composed of 21% PEG 3350 (Fluka) and 0.2 M Na^+/K^+ L-tartrate, and crystallized using the hanging-drop vapor diffusion technique. After 3 days, grown crystals were soaked in mother liquor supplemented with the inhibitor **7a** (10 mM final concentration of the inhibitor) for 20 hours. Crystals used for X-ray data collection were briefly transferred in reservoir solution supplemented with 22% glycerol and flash-frozen in liquid nitrogen. Crystallographic data obtained in this project were collected at 100 K on SOLEIL beamline PROXIMA1.

Structure determination, model building and refinement

Crystallographic data were processed and scaled using HKL2000[54]. Since the crystals of the smHDAC8/7a complex belonged to the same space group (P1) and had the same unit cell as native smHDAC8 crystals[36], only rigid-body refinement was used to adapt to the slight differences in unit cell constants using Phenix[55]. The initial model was refined through several cycles of manual building using Coot[56] and automated refinement with Phenix[55] and Buster[57]. The final model was validated using tools provided in Coot[56]. Visualization of structural data was done with Pymol[58], and two-dimensional diagram summarizing molecular interation between inhibitor **7a** and smHDAC8 enzyme was prepared with the help of LigPlot program[59]. Atomic coordinates and structure factors of the **7a**/smHDAC8 complex were deposited in the Protein Data Bank under the PDB ID code 5FUE.

AUTHOR INFORMATION

Corresponding author * Phone: +493455525040. E-mail: wolfgang.sippl@pharmazie.uni-halle.de

ACKNOWLEDGMENTS

This work and the authors of this manuscript received funding from the European Union's Seventh Framework Program for research, technological development and demonstration under grant agreements nos. 241865 (SEtTReND) and 602080 (A-ParaDDisE). We thank Karin Schmidtkunz, Simone Kniesa, Anja Kuberski and Inka Negwer for technical assistance. The work of CR and MM was supported by institutional funds from the Centre National de la Recherche Scientifique (CNRS), the Institute National de la Santé et de la Recherche Médicale (INSERM), and the Université de Strasbourg. The work of JL and RP was supported by institutional funds from the CNRS, the Institut Pasteur de Lille and the Université de Lille. This work was supported by the French Infrastructure for Integrated Structural Biology (FRISBI) ANR-10-INSB-05-01, and Instruct as part of the European Strategy Forum on Research Infrastructures (ESFRI). Work on human HDAC8 is supported by the Deutsche Forschungsgemeinschaft (DFG; MJ (Ju295/13-1), WS (Si868/13-1). MM, TBS, SD and CR thank members of SOLEIL for the use of their beamline facilities and for help during data collection.

ABBREVIATIONS USED

aq., aqueous; Boc, *tert*-butyloxycarbonyl; Boc_2O, di-tert-butyl dicarbonate; PyBOP, benzotriazol-1-yl-oxytripyrrolidinophosphonium hexafluorophosphate; $CDCl_3$, deuterated chloroform; CEF, chloro ethyl formiate; $CHCl_3$, chloroform; DCC, dicyclohexylcarbodiimide; DIPEA, di-isopropyl ethylamine; DMF, N,N-dimethylformamide; dDMSO, deuterated dimethyl sulfoxide; EtOAc, ethyl acetate; Et_3N, tri ethylamine; eq., equivalent; MeOH, methanol; $Na(AcO)_3BH$,sodium triacetoxy borohydride; n.a., not active; n.d., not determined;

NH_2OTHP, *O*-(tetrahydro-2*H*-pyran-2-yl)hydroxylamine; smHDAC8, *Schistosoma mansoni* histone deacetylase 8; $SOCl_2$, thionylchloride; sol., solution; t-BuOH, *tert*-butanol; TEA, triethyl amine; TFA, trifluoracetic acid; THF, tetrahydrofuran; TLC, thin layer chromatography; ZBG, zinc binding group

TABLE OF CONTENT GRAPHICS

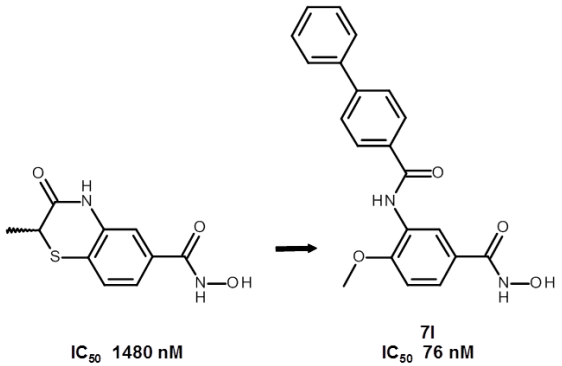

IC_{50} 1480 nM

7l
IC_{50} 76 nM

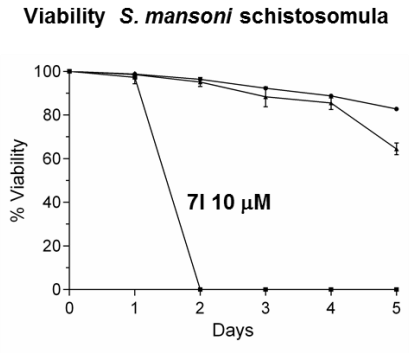

REFERENCES

(1) Hotez, P. J.; Kamath, A. Neglected Tropical Diseases in Sub-Saharan Africa: Review of Their Prevalence, Distribution, and Disease Burden. *PLoS Negl. Trop. Dis.* **2009**, *3*, e412.

(2) Brown, M. Schistosomiasis. *Clin. Med.* **2011**, *11*, 479–482.

(3) Ross, A. G.; Bartley, P. B.; Sleigh, A. C.; Olds, G. R.; Li, Y.; Williams, G. M.; McManus, D. P. Schistosomiasis. *N. Engl. J. Med.* **2002**, *346*, 1212–1220.

(4) Gray, D. J.; Ross, A. G.; Li, Y.-S.; McManus, D. P. Diagnosis and Management of Schistosomiasis. *BMJ* **2011**, *342*, d2651.

(5) WHO. Weekly Epidemiological Record Relevé Épidémiologique Hebdomadaire. **2015**, *376*, 25–32.

(6) Dömling, A.; Khoury, K. Praziquantel and Schistosomiasis. *Chem. Med. Chem*. **2010**, *5*, 1420–1421.

(7) Ismail, M.; Botros, S.; Metwally, A.; William, S.; Farghally, A.; Tao, L.; Day, T. I. M. A.; Bennett, J. L. Resistance To Praziquantel : Direct Evidence From *Schistosoma mansoni* Isolated From Egyptian Villagers. *Am. J. Trop. Med. Hyg.* **1999**, *60*, 932–935.

(8) Doenhoff, M. J.; Kusel, J. R.; Coles, G. C.; Cioli, D. Resistance of *Schistosoma mansoni* to Praziquantel: Is There a Problem? *Trans. R. Soc. Trop. Med. Hyg.* **2002**, *96*, 465–469.

(9) Webster, J. P.; Molyneux, D. H.; Hotez, P. J.; Fenwick, A. The Contribution of Mass Drug Administration to Global Health: Past, Present and Future. *Philos. Trans. R. Soc. Lond. B Biol. Sci.* **2014**, *369*, 20130434.

(10) Doenhoff, M. J.; Cioli, D.; Utzinger, J. Praziquantel: Mechanisms of Action, Resistance and New Derivatives for Schistosomiasis. *Curr. Opin. Infect. Dis.* **2008**, *21*, 659–667.

(11) Marek, M.; Oliveira, G.; Pierce, R. J.; Jung, M.; Sippl, W.; Romier, C. Drugging the Schistosome Zinc-Dependent HDACs: Current Progress and Future Perspectives. *Futur. Med. Chem.* **2015**, *7*, 783–800.

(12) Hotez, P. J.; Pecoul, B. "Manifesto" for Advancing the Control and Elimination of Neglected Tropical Diseases. *PLoS Negl. Trop. Dis*. **2010**, *4*, e718.

(13) Schäfer, S.; Jung, M. Chromatin Modifications as Targets for New Anticancer Drugs. *Arch. Pharm.* **2005**, *338*, 347–357.

(14) Pierce, R. J.; Dubois-Abdesselem, F.; Lancelot, J.; Andrade, L.; Oliveira, G.Targeting Schistosome Histone Modifying Enzymes for Drug Development. *Curr. Pharm. Des.* **2012**, *18*, 3567–3578.

(15) Andrews, K. T.; Haque, A.; Jones, M. K. HDAC Inhibitors in Parasitic Diseases. *Immunol. Cell Biol.* **2012**, *90*, 66–77.

(16) Ouaissi, M.; Ouaissi, A. Histone Deacetylase Enzymes as Potential Drug Targets in Cancer and Parasitic Diseases. *J. Biomed. Biotechnol.* **2006**, *2006*, 13474.

(17) Grunstein, M. Histone Acetylation in Chromatin Structure and Transcription. *Nature* **1997**, *389*, 349–352.

(18) Simone, C.; Peserico, A. Physical and Functional HAT/HDAC Interplay Regulates Protein Acetylation Balance. *J. Biomed. Biotechnol.* **2011**, *2011*, 371832.

(19) Yang, X. J.; Seto, E. The Rpd3/Hda1 Family of Lysine Deacetylases: From Bacteria and Yeast to Mice and Men. *Nat. Rev. Mol. Cell. Biol.* **2009**, *9*, 206–218.

(20) North, B. J.; Verdin, E. Sirtuins: Sir2-Related NAD-Dependent Protein Deacetylases. *Genome Biol.* **2004**, *5*, 224.

(21) Cho, Y. S.; Whitehead, L.; Li, J.; Chen, C. H. T.; Jiang, L.; Vögtle, M.; Francotte, E.; Richert, P.; Wagner, T.; Traebert, M.; Lu, Q.; Cao, X.; Dumotier, B.; Fejzo, J.; Rajan, S.; Wang, P.; Yan-Neale, Y.; Shao, W.; Atadja, P.; Shultz, M. Conformational Refinement of Hydroxamate-Based Histone Deacetylase Inhibitors and Exploration of 3-Piperidin-3-Ylindole Analogues of Dacinostat (LAQ824). *J. Med. Chem.* **2010**, *53*, 2952–2963.

(22) Marks, P.; Rifkind, R. A.; Richon, V. M.; Breslow, R.; Miller, T.; Kelly, W. K. Histone Deacetylases and Cancer: Causes and Therapies. *Nat. Rev. Cancer* **2001**, *1*, 194–202.

(23) Ito, K.; Ito, M.; Elliott, W. M.; Cosio, B.; Caramori, G.; Kon, O. M.; Barczyk, A.; Hayashi, S.; Adcock, I. M.; Hogg, J. C.; Barnes, P. J. Decreased Histone Deacetylase Activity in Chronic Obstructive Pulmonary Disease. *N. Engl. J. Med.* **2005**, *352*, 1967–1976.

(24) Mukherjee, P.; Pradhan, A.; Shah, F.; Tekwani, B. L.; Avery, M. A. Structural Insights into the Plasmodium Falciparum Histone Deacetylase 1 (PfHDAC-1): A Novel Target for the Development of Antimalarial Therapy. *Bioorg. Med. Chem.* **2008**, *16*, 5254–5265.

(25) Giannini, G.; Cabri, W.; Fattorusso, C.; Rodriquez, M. Histone Deacetylase Inhibitors in the Treatment of Cancer: Overview and Perspectives. *Future Med. Chem.* **2012**, *4*, 1439–1460.

(26) Marks, P. A.; Breslow, R. Dimethyl sulfoxide to vorinostat: development of this histone deacetylase inhibitor as an anticancer drug. *Nature Biotechnology.* **2007***,* 25, 84 - 90

(27) Balasubramanian, S.; Ramos, J.; Luo, W.; Sirisawad, M.; Verner, E.; Buggy, J.J. A novel histone deacetylase 8 (HDAC8)-specific inhibitor PCI-34051 induces apoptosis in T-cell lymphomas. *Leukemia.* **2008**, 22, 1026 - 1034

(28) Suzuki, T.; Ota, Y.; Ri, M.; Bando, M.; Gotoh, A.; Itoh, Y.; Tsumoto, H.; Tatum, P. R.; Mizukami, T.; Nakagawa, H.; Iida, S.; Ueda, R.; Shirahige, K.; Miyata, N. Rapid Discovery of Highly Potent and Selective Inhibitors of Histone Deacetylase 8 Using Click Chemistry to Generate Candidate Libraries. *J. Med. Chem.* **2012**, 55, 9562 - 9575

(29) Huang, W. J.; Wang, Y. C.; Chao, S. W.; Yang, C. J.; Chen, L. C.; Lin, M. H.; Hou, W. C.; Chen, M. Y.; Lee, T. L.; Yang, P.; Chang, C. I. Synthesis and biological evaluation of ortho-aryl N-hydroxycinnamides as potent histone deacetylase (HDAC) 8 isoform-selective inhibitors. *ChemMedChem*. **2012**, 7, 1815 - 1824

(30) Suzuki, T.; Muto, N.; Bando, M.; Itoh, Y.; Masaki, A.; Ri, M.; Ota, Y.; Nakagawa, H.; Iida, S.; Shirahige, K.; Miyata, N. Design, synthesis, and biological activity of NCC149 derivatives as histone deacetylase 8-selective inhibitors. *ChemMedChem.* **2014**, 9, 657 - 664

(31) Andrews, K. T.; Walduck, A.; Kelso, M. J.; Fairlie, D. P.; Saul, A.; Parsons, P. G. Anti-Malarial Effect of Histone Deacetylation Inhibitors and Mammalian Tumour Cytodifferentiating Agents. *Int. J. Parasitol.* **2000**, *30*, 761–768.

(32) Oger, F.; Dubois, F.; Caby, S.; Noël, C.; Cornette, J.; Bertin, B.; Capron, M.; Pierce, R. J. The Class I Histone Deacetylases of the Platyhelminth Parasite *Schistosoma mansoni. Biochem. Biophys. Res. Commun.* **2008**, *377*, 1079–1084.

(33) Dubois, F.; Caby, S.; Oger, F.; Cosseau, C.; Capron, M.; Grunau, C.; Dissous, C.; Pierce, R. J. Histone Deacetylase Inhibitors Induce Apoptosis, Histone Hyperacetylation and up-Regulation of Gene Transcription in *Schistosoma mansoni*. *Mol. Biochem. Parasitol.* **2009**, *168*, 7–15.

(34) Lancelot, J.; Caby, S., Dubois-Abdesselem, F.; Vanderstraete, M.; Trolet, J.; Oliveira, G.; Bracher, F.; Jung, M.; Pierce, R.J. Schistosoma mansoni sirtuins: characterization and potential as chemotherapeutic targets. *PLoS Negl. Trop. Dis*. **2003**, 7, e2428.

(35) Nakagawa, M.; Oda, Y.; Eguchi, T.; Aishima, S.-I.; Yao, T.; Hosoi, F.; Basaki, Y.; Ono, M.; Kuwano, M.; Tanaka, M.; Tsuneyoshi, M. Expression Profile of Class I Histone Deacetylases in Human Cancer Tissues. *Oncol. Rep.* **2007**, *18*, 769–774.

(36) Marek, M.; Kannan, S.; Hauser, A. T.; Moraes Mourão, M.; Caby, S.; Cura, V.; Stolfa, D. A.; Schmidtkunz, K.; Lancelot, J.; Andrade, L.; Renaud, J. P.; Oliveira, G.; Sippl, W.; Jung, M.; Cavarelli, J.; Pierce, R. J.; Romier, C. Structural Basis for the Inhibition of Histone Deacetylase 8 (HDAC8), a Key Epigenetic Player in the Blood Fluke *Schistosoma mansoni*. *PLoS Pathog.* **2013**, *9*, e1003645.

(37) Stolfa, D.; Marek, M.; Lancelot, J.; Hauser, A.-T.; Walter, A.; Leproult, E.; Melesina, J.; Rumpf, T.; Wurtz, J.-M.; Cavarelli, J.; Sippl, W.; Pierce, R. J.; Romier, C.; Jung, M. Molecular Basis for the Antiparasitic Activity of a Mercaptoacetamide Derivative That Inhibits Histone Deacetylase 8 (HDAC8) from the Human Pathogen *Schistosoma mansoni. J. Mol. Biol.* **2014**, *426*, 3442–3453.

(38) Kannan, S.; Melesina, J.; Hauser, A.; Chakrabarti, A.; Heimburg, T.; Schmidtkunz, K.; Walter, A.; Marek, M.; Pierce, R. J.; Romier, C.; Jung, M.; Sippl, W. Discovery of Inhibitors of *Schistosoma mansoni* HDAC8 by Combining Homology Modeling, Virtual Screening, and in Vitro Validation. *J. Chem. Inf. Model.* **2014**, *54*, 3005–3019.

(39) Chakrabarti, A.; Oehme, I.; Witt, O.; Oliveira, G.; Sippl, W.; Romier, C.; Pierce, R. J.; Jung, M. HDAC8: A Multifaceted Target for Therapeutic Interventions. *Trends Pharmacol. Sci.* **2015**, *36*, 481-92.

(40) Rodrigues, D. A.; Ferreira-Silva, G. À.; Ferreira, A. C. S.; Fernandes, R. A.; Kwee, J. K.; Sant'Anna, C. M. R.; Ionta, M.; Fraga, C. A. M. Design, Synthesis, and Pharmacological Evaluation of Novel N‑Acylhydrazone Derivatives as Potent Histone Deacetylase 6/8 Dual Inhibitors. *J. Med. Chem* **2016**, Article ASAP DOI: 10.1021/acs.jmedchem.5b01525, Publication Date (Web): December 24, 2015

(41) Wang, L.; Kofler, M.; Brosch, G.; Melesina, J.; Sippl, W.; Martinez, E. D.; Easmon, J. 2-Benzazolyl-4-Piperazin-1-Ylsulfonylbenzenecarbo-hydroxamic Acids as Novel Selective Histone Deacetylase-6 Inhibitors with Antiproliferative Activity. *PLoS ONE* **2015**, 10, e0134556.

(42) Lobera, M.; Madauss, K. P.; Pohlhaus, D. T.; Wright, Q. G.; Trocha, M.; Schmidt, D. R.; Baloglu, E.; Trump, R. P.; Head, M. S.; Hofmann, G. A.; Murray-Thompson, M.; Schwartz, B.; Chakravorty, S.; Wu, Z.; Mander, P. K.; Kruidenier, L.; Reid, R. A.; Burkhart, W.; Turunen, B. J.; Rong, J. X.; Wagner, C.; Moyer, M. B.; Wells, C.; Hong,X.; Moore, J. T.; Williams, J. D.; Soler, D.; Ghosh, S.; Nolan, M. A. Selective class IIa histone deacetylase inhibition via a nonchelating zinc-binding group. *Nat. Chem. Biology* **2013**, *9*, 319–325.

(43) Olson, D. E.; Wagner, F. F.; Kaya, T.; Gale, J. P.; Aidoud, N.; Davoine, E. L.; Lazzaro, F.; Weïwer, M.; Zhang, Y. L.; Holson, E. B. Discovery of the First Histone Deacetylase 6/8 Dual Inhibitors. *J. Med. Chem.* **2013**, *56* , 4816–4820.

(44) Tang, W.; Luo, T.; Greenberg, E. F.; Bradner, J. E.; Schreiber, S. L. Discovery of histone deacetylase 8 selective inhibitors. *Bioorg. Med. Chem. Letters* **2011**, *21* , 2601–2605.

(45) KrennHrubec, K.; Marshall, B. L.; Hedglin, M.; Verdin, E.; Ulrich, S. Ma. Design and evaluation of 'Linkerless' hydroxamic acids as selective HDAC8 inhibitors. *Bioorg. Med. Chem. Letters* **2007**, *17*, 2874–2878

(46) Panic, G.; Flores, D.; Ingram-Sieber, K.; Keiser, J. Fluorescence/luminescence-based markers for the assessment of *Schistosoma mansoni* schistosomula drug assays. *Parasit. Vectors* **2015**, 8, 624.

(47) Choudhary, C.; Kumar, C.; Gnad, F.; Nielsen, M. L.; Rehman, M.; Walther, T. C.; Olsen, J. V; Mann, M. Lysine Acetylation Targets Protein Complexes and Co-Regulates Major Cellular Functions. *Science* **2009**, *325*, 834–840.

(48) Eswar, N.; Webb, B.; Marti-Renom, M. A.; Madhusudhan, M. S.; Eramian, D.; Shen, M. Y.; Pieper, U.; Sali, A. Comparative Protein Structure Modeling Using Modeller. *Curr. Protoc. Bioinforma.* **2006**, *Chapter 5*, Unit 5 6.

(49) Suite 2012, Maestro Version 9.3, Protein Preparation Wizard, Epik Version 2.3, Glide Version 5.8, Schrödinger, LLC, New York, NY, **2012**.

(50) Marxer, M.; Ingram, K.; Keiser, J. Development of an in Vitro Drug Screening Assay Using *Schistosoma haematobium* schistosomula. *Parasit. Vectors* **2012**, *5*, 165.

(51) Ramalho-Pinto, F. J.; Gazzinelli, G.; Howells, R. E.; Mota-Santos, T.; Figueiredo, E.; Pellegrino, J. *Schistosoma mansoni*: Defined System for Stepwise Transformation of Cercaria to Schistosomule in Vitro. *Exp. Parasitol.* **1974**, *36*, 360–372.

(52) Vanderstraete, M.; Gouignard, N.; Cailliau, K.; Morel, M.; Lancelot, J.; Bodart, J. F.; Dissous, C. Dual Targeting of Insulin and Venus Kinase Receptors of *Schistosoma mansoni* for Novel Anti-Schistosome Therapy. *PLoS Negl. Trop. Dis.* **2013**, *7*, e2226.

(53) Smithers, S. R.; Terry, R. J. The Infection of Laboratory Hosts with Cercariae of *Schistosoma mansoni* and the Recovery of the Adult Worms. *Parasitology* **1965**, *55*, 695–700.

(54) Otwinowski, Z.; Minor, W. Processing of X-ray diffraction data collected in oscillation mode. *Methods Enzymol.* **1997**, 276, 307–326.

(55) Adams, P. D.; Afonine, P.V.; Bunko´czi, G.; Chen, V. B.; Davis, I.W. PHENIX: A comprehensive Python-based system for macromolecular structure solution. *Acta Crystallogr. D Biol. Crystallogr*. **2010**, 66, 213–221.

(56) Emsley, P.; Cowtan, K. Coot: model-building tools for molecular graphics. *Acta Crystallogr. D Biol. Crystallogr*. **2004**, 60, 2126–2132.

(57) Blanc, E.; Roversi, P.; Vonrhein, C.; Flensburg, C.; Lea, S.M.. Refinement of severely incomplete structures with maximum likelihood in BUSTER-TNT. *Acta Crystallogr. D Biol. Crystallogr*. **2004**, 6, 2210–2221.

(58) The PyMOL Molecular Graphics System, Version 1.7.4 Schrödinger, LLC.

(59) Wallace, A. C.; Laskowski, R. A.; Thornton, J. M. LIGPLOT: a program to generate schematic diagrams of protein-ligand interactions. *Protein Eng.* **1996**, 8, 127-134.